NONLINEAR FIBER ELEMENT ANALYSIS OF A REINFORCED CONCRETE SHEAR WALL SUBJECTED TO EARTHQUAKE RECORDS[*]

H. BEIRAGHI[1**], A. KHEYRODDIN[2] AND M. A. KAFI[3]

[1]Dept. of Civil Engineering, Mahdishahr Branch, Islamic Azad University, Mahdishahr, I. R. of Iran
Email: H_beiraghi@yahoo.com
[2,3]Civil Engineering Faculty, Semnan University, Semnan, I. R. of Iran
[2]Dept. of Civil Engineering and Applied Mechanics, University of Texas, Arlington, TX, USA

Abstract– Verifying the behavior of shear walls in a tall building requires reliable response results. This paper examined nonlinear fiber element modeling of a slender reinforced concrete shear wall during large-scale shaking table testing. The goal was to understand and validate the inelastic responses given by fiber models using time history analysis. Reasonable agreement was found between the numerical and experimental responses. It was demonstrated that the spread of the second plastic hinge into the upper level of a shear wall can be adequately captured using fiber modeling in response to the effect of higher modes. The parameters of damping, shear stiffness, axial load, concrete strength, longitudinal reinforcement ratio and mass were examined. The shear and moment demand distribution were sensitive to axial loading, mass and reinforcement ratio. The drift distribution along the height, rotation, and top horizontal displacement were also investigated and it was found that the sole use of Rayleigh damping did not produce accurate responses. Increasing longitudinal reinforcement did not prevent nonlinear flexural behavior in the upper levels.

1. INTRODUCTION

Structures require sufficient nonlinear deformation capacity, stiffness and strength to resist strong ground motion caused by earthquake loading. Ductile reinforced concrete (RC) shear walls experience yielding of flexural reinforcement in the plastic hinge regions that control strength, deformation and energy dissipation [1-3].

The best way to predict seismic performance of a structural system is to perform nonlinear time history analysis of a properly developed analytical model. The uncertainties associated with site-specific ground motion and analytical modeling parameters make it difficult to justify the effort associated with detailed modeling and analysis [4-6].

Fiber element models are more common than finite element models because they can predict the inelastic flexural response of RC shear walls in detail and they require less computational effort [7-10]. Utilizing fiber models with detailed geometrical descriptions of the wall and suitable materials is increasing continually. To define material properties such as longitudinal reinforcement, confined and unconfined concrete specifications is important [11]. Computer programs such as Perform-3D and Seismosoft used for seismic design of RC structures employ fiber element models [12, 13]. In the fiber model of a shear wall, the cross-section is discretized into longitudinal fibers with a definite relationship between concrete and reinforcing steel. Perform-3D has been used in numerous studies to investigate the nonlinear behavior of RC shear walls in tall buildings [14-18].

Orakcal et al. [1, 19] studied the capability of current modeling approaches to capture the cyclic behavior of slender RC walls under combined flexural bending and axial loading. They considered a multiple-vertical-line-element model that was similar to some fiber element models for walls subjected to cyclic loading. The result of the fiber model of a large-scale concrete shear wall was in good agreement with laboratory data gathered under cyclic loading. Furthermore, fiber element modeling of large-scale shaking table data for a slender RC shear wall showed good agreement between the numerical and experimental results [20].

Retaining the lateral force resistance within the elastic range during a severe earthquake is costly, so codes recommend the use of reduced lateral loads and permit the development of nonlinear behavior in some regions of the structural system during strong ground motion. Nonlinear flexural deformation in cantilever shear walls occurs in regions recognized as plastic hinges. Traditionally, the development of one plastic hinge at the base of a wall is favorable [21].

Details of reinforcement for the plastic hinge regions are important to ensuring that deformation has a low probability of exceeding capacity. Codes prescribe requirements that ensure a degree of ductility in the potential plastic hinge regions. Capacity design used by EC8, NZS-3101 and CSA also ensure elastic behavior in regions other than plastic hinges. These codes consider the effect of higher modes [22-24]. Rodriguez et al. [25] found that inelastic response at the base of a cantilever wall decreased the response of the first mode, but did not affect higher modes. Panneton et al. [26] and Priestley et al. [27] reported similar findings. As will be demonstrated, preventing the spread of plasticity into the upper levels of a cantilever shear wall designed according to code cannot be easily achieved using an increased longitudinal reinforcement ratio ($\frac{As}{Ag}$) in which As is the longitudinal reinforcement cross-section area and Ag is the gross area of a cross-section of the shear wall.

To the knowledge of the authors, only one experimental study was found that reported nonlinear responses at the upper level of a shear wall. Shaking table testing under design-level base motion by Ghorbanirenani et al. [28] demonstrated inelastic flexural response at the wall base (expected) and at the upper level (unexpected). This behavior resulted from higher mode responses under high-frequency motion. Historical evidence confirms plastic hinge formation at the intermediate height of shear walls [29, 30].

The current investigation generated a constitutive RC shear wall model using nonlinear fiber models in Perform-3D to verify the experimental data of large-scale shaking table testing. The results of the numerical model and experimental study were found to be significantly consistent. Development of an inelastic flexural response above the base of a RC shear wall was accurately captured using nonlinear time history analysis. A subsequent parametric study investigated the responses and studied modal damping, axial load, mass, longitudinal reinforcement ratio, concrete strength and shear stiffness. The outcomes of this research can increase insight into the performance of RC shear walls subjected to earthquake loading by employing fiber element models.

2. SHAKING TABLE TEST OF A SHEAR WALL

Results of experimental testing of a RC shear wall by Ghorbanirenani et al. [28] were used to verify the model results. The test program used unidirectional shaking table testing. The model had the characteristics of an 8-story RC shear wall. The total height of the wall was 9.0-m, the story height was 1.125-m and the scale factor was 0.429. The length of the wall was 1.4-m up to the sixth level and 1.2-m above this level. This decrease at the sixth floor was designed to accurately match the bending moment demand at that location. Wall thickness was 80 mm. A simulated ground motion time history was modified to match the design spectrum obtained from Canadian code [28]. The 5% damped spectrum of

the design level earthquake ground motion is shown in Fig. 1 and the motion time history is depicted in Fig. 2.
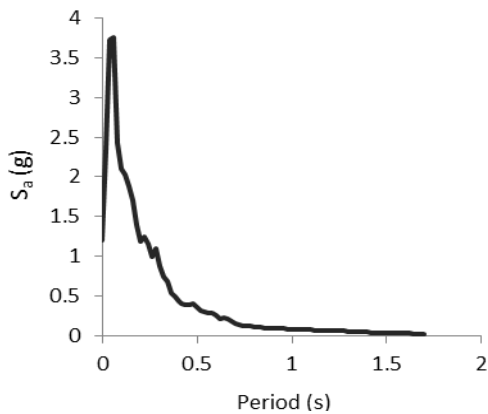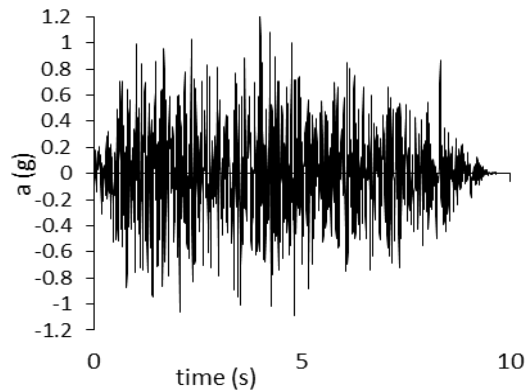

Fig. 1. 5% damped acceleration spectrum

Fig. 2. Ground motion history

All acceleration and time values are in accordance with the scale of the model. The concrete compression strength was 30 MPa as in the laboratory testing. A vertical load of 90.7 KN was applied to the top of the wall to represent the axial load. Adding the self-weight of the wall makes the axial force (Pc) at the wall base 2.7% Agf_c', where Ag is the gross area of the cross-section of the shear wall and f_c' is the nominal compressive strength of the wall. A plastic hinge formation was reported at the base, as expected, and in the upper level due to the effect of the higher modes. The seismic weight at each story was approximately 62 KN. Details of the test setup and shear wall cross sections are shown in Fig. 3 [28]. During the test, horizontal displacements, accelerations and inertia forces were directly measured at every level by using instrumentation. Story shear and overturning bending moments were obtained from the measured forces. Figure 3 shows the steel plates used as seismic mass that has been connected to the wall by using horizontal struts in each floor. Load cells were used between wall and strut to measure the horizontal inertia force at the floor levels. Besides, accelerometers were also used at every floor to evaluate the inertia forces from the wall self-weight. Induced lateral seismic force in each floor can be calculated from multiplying the floor mass by measured acceleration.
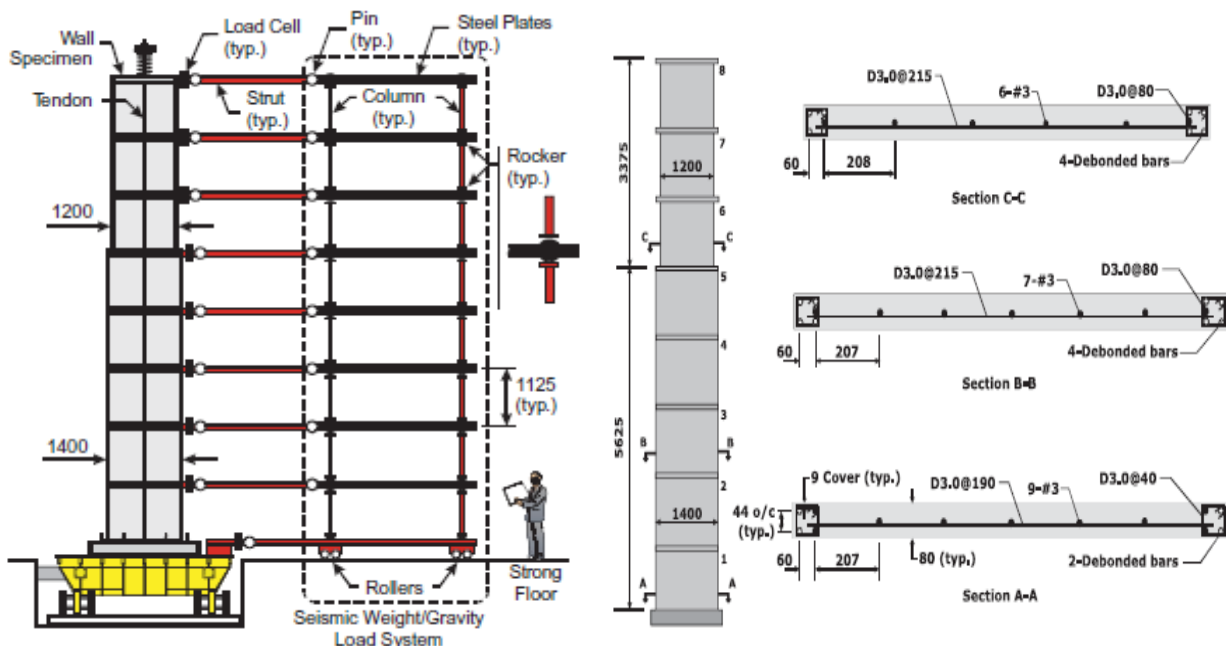

Fig. 3 Test specimen and cross-sections of the tested wall [10]

Table 1 gives the maximum horizontal displacement of the top of the wall (Δ_r), first level rotation (θ_b), sixth level rotation (θ_6), sixth story drift (Dr_6) and shear deformation of the first story (γ) from experimental testing and numerical models.

3. NONLINEAR SIMULATION OF THE PROTOTYPE WALL

As mentioned earlier, fiber models have been used extensively to predict the behavior of the RC walls subjected to both static and dynamic loads because they have distinct advantages over lumped-plasticity beam-column models. Unlike lumped-plasticity elements, fiber elements can predict neutral axis migration during lateral loading and the effect of variable axial loading on wall stiffness and strength [31]. In the concentrated plastic hinge models, the plasticity is forced to occur in a distinct region, while in the fiber model the plasticity can extend anywhere.

The dynamic nonlinear structural behavior of the shear wall was calculated using the fiber element model implemented in PERFORM-3D [12]. In this software, shear wall elements are available to model RC walls. Each element has 4 nodes and 24 degrees of freedom. The fiber cross-section contains vertical steel and concrete fibers. In each wall element, Axis 2 is vertical, Axis 3 is horizontal, and Axis 1 is normal to the plane of the wall element. The cross section of the shear wall using the fiber model is depicted in Fig. 4. The behavior of the concrete and steel was represented by stress-strain constitutive law. To model the wall, one element over the story height was used as recommended by Powell [32]. The "shear wall, inelastic section" software component was used to define the wall section. Out-of-plane bending was assumed to be linear. Vertical in-plane behavior is considerably more important than transverse (horizontal) behavior. In the vertical direction, wall elements can be inelastic in bending and/or shear. In the transverse in-plane direction, the behavior is assumed to be elastic and secondary. As the vertical fibers yield and/or crack in the inelastic fiber section, the effective centroidal axis shifts [12]. The material properties are described below.
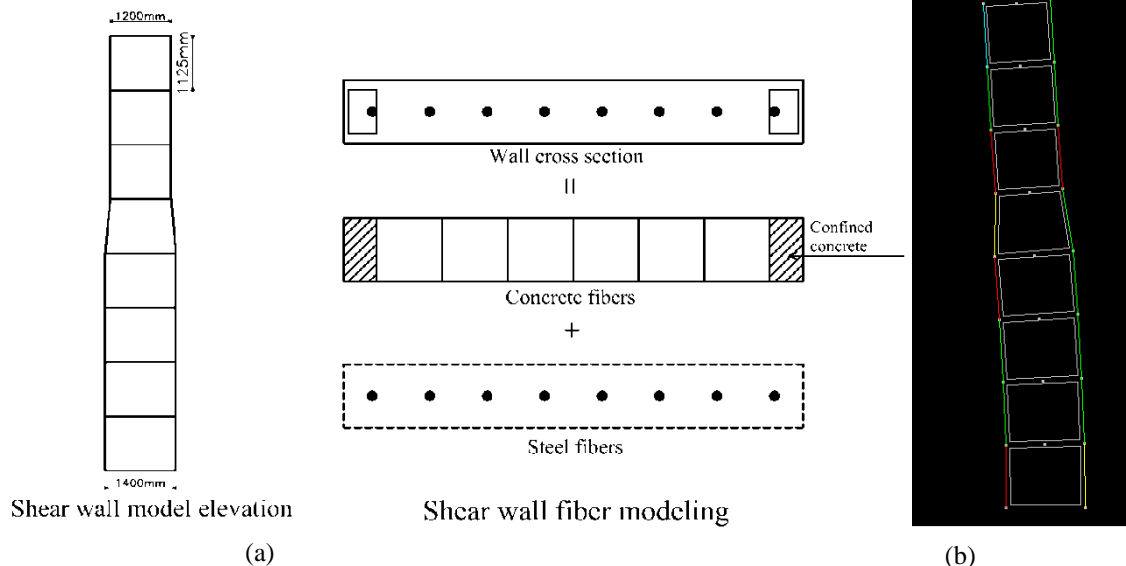

Fig. 4. (a) Fiber model representation of the shear wall; (b) Snapshot view of the shear wall elements during vibration (the red color shows the plasticity extension.

a) Constitutive material relations

In Perform-3D, 8 concrete fibers and 8 reinforced fibers were employed along the height to model the shear wall. For the concrete fiber elements, confined concrete was used to model the boundary zones and unconfined concrete was used to model the remaining portions. Numerous studies have been carried out

on the stress-strain relationship of concrete confined by transverse reinforcement under compression. Investigations and laboratory tests have shown that if the compression zone of a concrete member is confined sufficiently by stirrup ties or spirals, the ductility of concrete is considerably enhanced and the member can sustain deformations of large curvature demand. The modified Kent and Park concrete model was used for modeling the material behavior of concrete under compression [33]. The formulations of the stress-strain relations of confined and unconfined concrete model are summarized here. The constitutive concrete model graph consists of an ascending part represented by a second-degree parabolic curve and a descending linear segment. The parabolic curve is expressed by Eqs. (1) and (2).

$$f_c = kf_c'[\frac{2\varepsilon_c}{k\varepsilon_0} - (\frac{\varepsilon_c}{k\varepsilon_0})^2] \tag{1}$$

$$k = 1 + \frac{\rho f_y}{f_c'} \tag{2}$$

Where ε_c is the longitudinal concrete strain, f_c' is the compressive strength of concrete, ε_0 is the strain of unconfined concrete corresponding to f_c', k is a confinement coefficient, f_y is the yielding strength of the horizontal reinforcement, and ρ is volumetric ratio of confining steel. For unconfined concrete, the parameter k is equal to one. More information has been explained in other references [33]. The strength of compression concrete was adapted from measured concrete properties in experimental test [28]. Figure 5 shows the used stress-strain curves of compression concrete and the confinement effect on the concrete behavior. The tensile strength of concrete was ignored. Since Perform-3D requires a description of the stress-strain relation of the concrete using four lines, four linear segments were drawn to approximate Kent-Park concrete behavior. The expected yield strength and ultimate strength of the longitudinal reinforcement were 455 and 706 MPa, respectively [28]. The stress-strain relationship of the steel bars is plotted in Fig. 5. The stiffness and strength degradation were further accounted for by specifying the energy degradation factors for steel. These factors are the ratios of the areas of the degraded to non-degraded hysteresis loops [34, 35].
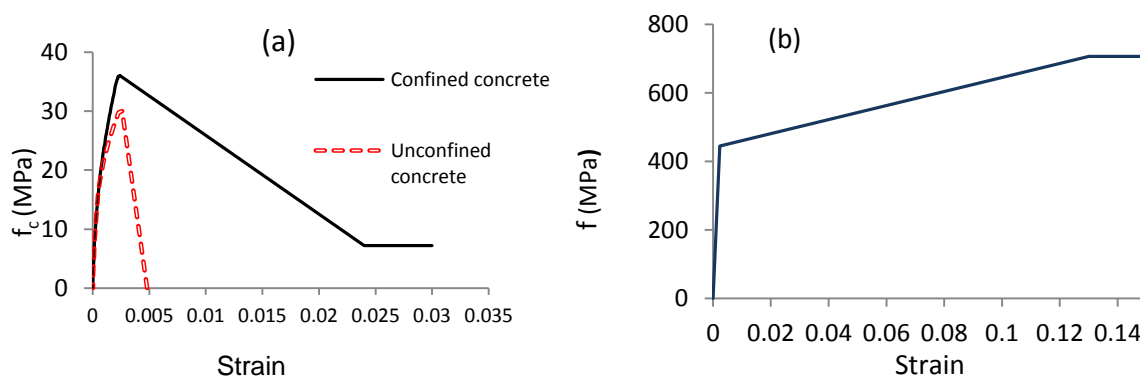

Fig. 5. (a) Confined and unconfined concrete stress-strain. (b) Steel bar stress-strain

b) Shear stiffness of the shear wall

In shear wall models, shear and flexural/axial behavior are uncoupled in Perform-3D. The 8-story RC shear wall was capacity designed so that shear did not control the lateral strength or energy dissipation. Elastic shear behavior is typically assumed in these elements, even when nonlinear flexural behavior is anticipated [11]. The time history of the longitudinal strain in the horizontal shear reinforcement of the experimental specimen indicated that the steel remained in the elastic range [28].

Shear behavior was modeled using linear shear stiffness. Cracking caused by earthquake loading decreases effective stiffness; to account for this, effective shear stiffness was used in the verification

study. No definitive rule exists to determine the effective shear stiffness of shear walls; different studies have recommended different values for RC walls. In ATC72, the typical value for shear stiffness can be as low as $(\frac{Gc.Ag}{10})$ to $(\frac{Gc.Ag}{20})$, where G_C is the shear modulus of un-cracked concrete and Ag is the wall gross area of the cross-section [31].

In the present study, $(\frac{Gc.Ag}{7})$ was employed for the first through fifth and eighth stories and $(\frac{Gc.Ag}{20})$ for the sixth and seventh stories. These values were selected by trial and error.

c) Axial load and mass modeling

Axial force was modeled using two nodal loads as point loads at each end of the top of the wall. The self-weight of the wall was considered to be part of the axial gravity load and the seismic load. The seismic mass was lumped at the center of mass at each story level. The effect of P-Delta was considered in the analysis.

d) Damping modeling

Nonlinear analysis has shown that the assumption of damping strongly affects the results [36]. The appropriate modeling of damping in nonlinear time history analysis is essential. Unsuitable modeling choices may lead to behaviors not representative of the real response of a structure caused primarily by numerical error, as shown in previous studies on the effect of damping modeling assumptions [37, 38]. Bernal stated that the use of Rayleigh damping may lead to excessive damping forces [39]. Hall concluded that when yielding occurs, Rayleigh damping may produce greater damping forces that result in non-conservative results [40]. Chopra believed that Rayleigh damping cannot be used unless similar damping mechanisms are provided throughout the structure [41]. The results from the test wall were in reasonable agreement with the numerical model using 2.5% modal damping for all modes plus 0.15% Rayleigh damping for the first and third modes.
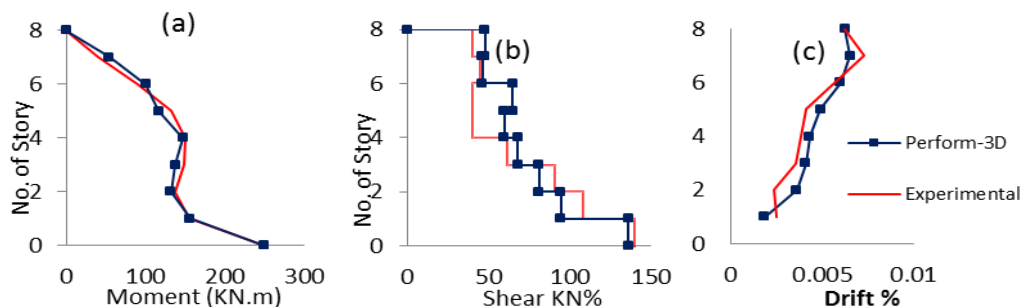

Fig. 6. Experimental and numerical responses: (a) moment distribution envelope;
(b) shear distribution envelope; (c) drift distribution envelope

4. NONLINEAR TIME HISTORY ANALYSIS

The final numerical model was found by trial and error and nonlinear time history analysis of the fiber element model was performed to verify the model behavior using the experimental results. Figure 6 shows the moment, shear and drift distribution envelopes from the tested wall and from the final verified fiber element model. This figure demonstrates that the moment demand from the numerical model along the wall height is in good agreement with the experimental data. The shape of the moment demand curve differs from the moment demand pattern obtained from elastic analysis. The reason for this is the significant contribution of the higher mode of vibration to the responses. The occurrence of a plastic hinge at the base decreases the first mode effect, but does not significantly decrease the effects of the higher modes. The base shear of the experimental and numerical models was about the same; however, they did not match in the upper levels. Shear amplification caused by the effect of higher modes in the testing data

was predicted by the fiber model used in the present study. For the drift demand outline in Fig. 6c, the overall trends of the two diagrams are roughly similar and the numerical results are very close to the experimental data.

Table 1. Peak Response Parameters measured by the test and resulted from the fiber model

		Δ_r (cm)	θ_b	θ_6	Dr_6	γ (10^-4)
	Experimental	32	0.0027	0.0023	0.006	7.8
	Perform-3D	34	0.0027	0.0024	0.006	7.9
Modal damping	5%	27	0.00185	0.00185	0.0048	8.3
	3%	29	0.0021	0.0021	0.005	7.9
	1%	47	0.0039	0.0029	0.0087	9
Rayleigh damping	5%	26	0.0012	0.00044	0.0042	2.9
	2.5%	29	0.0014	0.0007	0.0047	4.5
	1%	40	0.0025	0.0011	0.0066	6
Axial load ratio ($Pc/A_g . f'_c$)	6%	39	0.0029	0.0024	0.007	12.5
	12%	36	0.0024	0.0016	0.007	12.5
	18%	33	0.0022	0.0014	0.0062	12.5
Mass	$\times 2$	36.5	0.0025	0.0053	0.0078	10.6
	$\times 3$	37.5	0.0022	0.0019	0.007	13
	$\times 0.5$	33	0.0019	0.0019	0.006	6.3
Reinforcement ratio (A_s/A_g)	$\times 2$	37	0.0024	0.0023	0.008	12
	$\times 3$	30	0.0018	0.0019	0.006	12
	$\times 0.5$	34	0.0035	0.0032	0.0067	8
Shear stiffness	$\times 0.5$	39	0.0031	0.0028	0.0084	15
	$\times 2$	34	0.0027	0.0025	0.0057	4.3
	$\times 4$	34	0.0027	0.0025	0.0056	2.1
f_c	$\times 2$	32	0.0023	0.0023	0.0054	5.8
	$\times 1.5$	30	0.0022	0.0022	0.0055	4.5
Upper reinforcement ratio (A_s/A_g)	$\times 2$	33	0.0026	0.002	0.0059	9
	$\times 3$	32	0.0024	0.002	0.006	10.7

Table 1 shows that Δ_r has been slightly overestimated. The θ_b and θ_6 values, shear deformation of the first story and the periods of the first, second and third modes in the testing data and numerical models are in good agreement. The yielding rotations of the base and sixth story from cross-section analysis were 0.0022 and 0.0018 rad, respectively. The values from both testing data and numerical analysis were 0.0027 and 0.0023 rad, respectively, it is evident that sixth level yielding occurred in addition to base yielding. The nonlinear fiber method was able to determine this occurrence.

5. PARAMETRIC STUDY USING VERIFIED NONLINEAR MODEL

a) Damping

For the purposes of this study, the main damping used in the fiber model was modal damping plus a small amount of Rayleigh damping. Figure 7 represents the effect of modal damping on moment, shear and drift demand. It is noted that the 2.5% Modal damping plus 0.15% Rayleigh damping scenario was selected as best for the fiber model.

Decreasing Modal damping to 1% caused an approximate 17% increase in base moment demand. Conversely, increasing Modal damping to 3.5% and 5%, caused 12% and 21% decrease in base moment demand respectively; thus, the effect of damping ratio on moment demand was modest. Similar results were found for base shear demand, as shown in Fig. 7. Decreasing the damping ratio from 2.5% to 1% increased upper level drift demand by 45%; however, when the modal damping value was greater than

2.5%, the decrease in drift was not as large. Increasing the modal damping values decreased rotation in the first and sixth stories and top displacement, and vice-versa (Table 1).
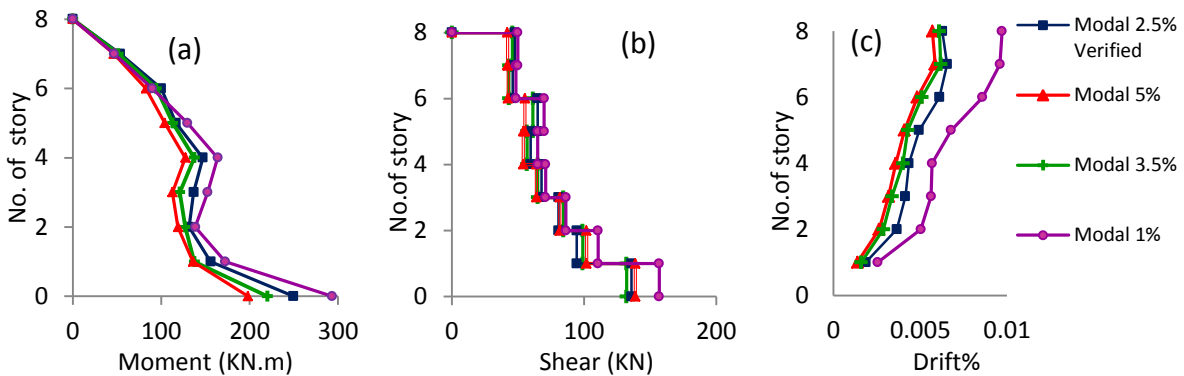

Fig. 7. Modal damping effect on: (a) moment demand distribution;
(b) shear demand distribution; (c) drift demand distribution

Several researchers have used only 2.5% Rayleigh damping for fiber element modeling of tall shear walls. The effect of the sole use of Rayleigh damping at 1%, 2.5% and 5% was investigated and the results are shown in Fig. 8. As seen, the result was underestimation in prediction of the upper level moments and rotations. Base moment prediction was underestimated at 2.5% Rayleigh damping and overestimated at 1%. It should be noted that Rayleigh damping could not predict the rotation of the sixth story or top displacement (Table 1). Additional testing of the effects of Rayleigh damping (not shown) did not provide satisfactory results. These findings agree with the results of previous studies [39].
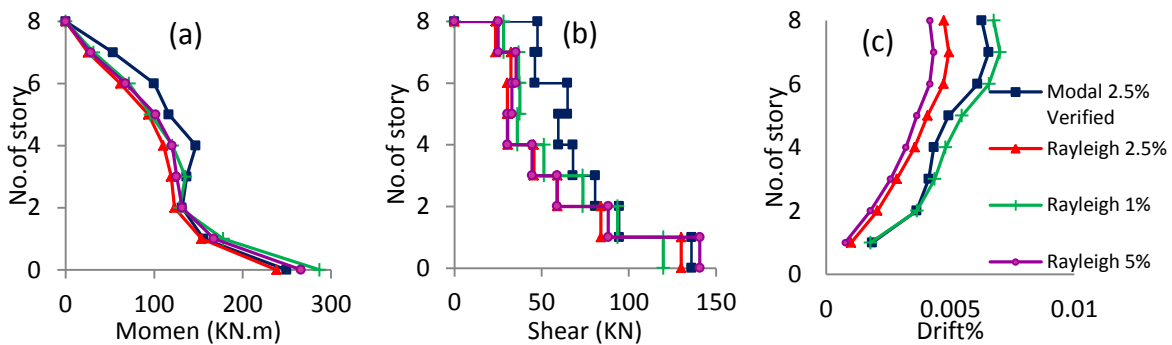

Fig. 8. Rayleigh damping effect on: (a) moment demand distribution;
(b) shear demand distribution; (c) drift demand distribution

b) Shear stiffness

In the fiber element model, shear deformation is considered to be linear elastic. The effect of shear stiffness was studied by multiplying the shear stiffness of each story by 0.5, 2 and 4 in the verified model. As shown in Fig. 9, changing the shear stiffness had little effect on the moment or shear demands. Multiplying the shear stiffness by 0.5 significantly increased upper story drift. Increasing shear stiffness had a small effect on story drift.

c) Axial loading

The ratio of axial load to Agf_c' in experimental testing was 2.7% at the wall base, which is a low axial load for walls and occurs mostly around stairways. The effect of increased axial loading is plotted in the Fig. 10. When the axial load ratio increased to 6%, 12% and 18%, the base moment demand increased about 32%, 57% and 73%, respectively. These results were roughly the same for each level. An increase in moment value is reasonable because, for a member with a small axial compression force, bending

moment capacity will increase as the axial load increases, which is according to the loading on shear demand. An increase in flexural moment demand along the height requiring increased lateral loading resulted in increased shear demand. This shows that shear force demand along the height of a cantilever wall can be larger than expected [41] because of the higher modes effect in the inelastic range. Figure 10b shows that dynamic amplification increased as axial loading increased.
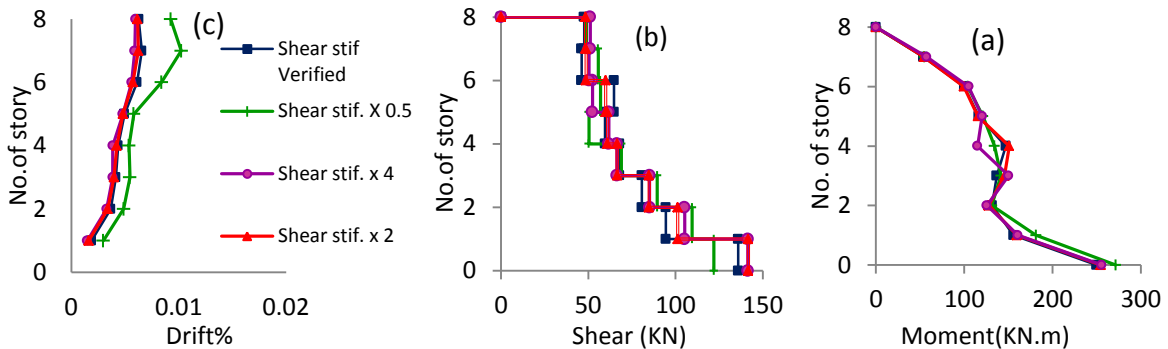

Fig. 9. Effect of shear stiffness values on: (a) moment demand distribution;
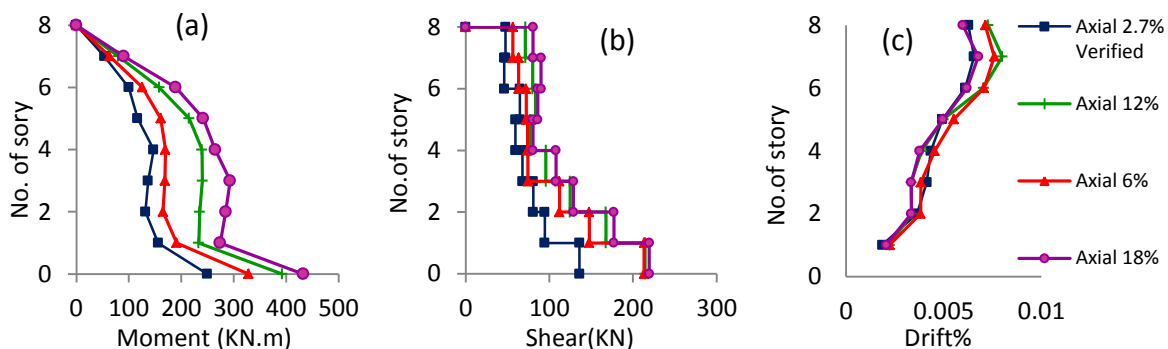(b) shear demand distribution; (c) drift demand distribution

Fig. 10. Effect of axial load ratio on: (a) moment demand distribution;
(b) shear demand distribution; (c) drift demand distribution.

Drift along the height in the model with different axial loading is depicted in Fig. 10c. It is evident that there was no uniform rule governing drift versus axial loading, probably because of the higher modes effect and the frequency content of the earthquake record. Increasing axial loading decreased rotation in the first and sixth levels and top displacement (Table 1).

d) Effect of mass

The amount of mass along the height of the shear wall can change the response. Figure 11 shows that doubling and tripling the model mass increased the base moment by 8% and 16%, respectively. When one-half the mass of the prototype shear wall was used, the base moment and base shear demand decreased about 20% and 25%, respectively. When the mass was doubled and tripled, base shear demand increased about 34% and 78%, respectively. Figure 11c demonstrates the effect of mass on drift. When the mass doubled, a rapid increase occurred in upper story drift due to nonlinear rotation in the upper levels. Further increases in mass did not increase drift at those levels. There was no simple correlation between mass quantity and drift which could be caused by frequency content of the base motion (Table 1).
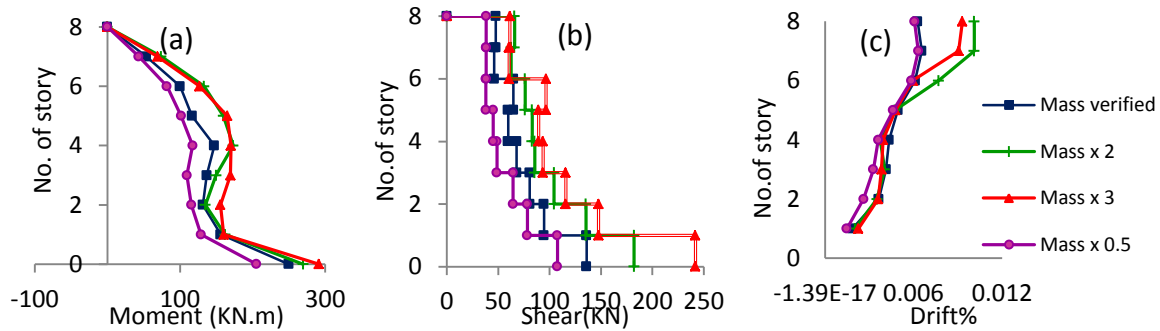
Fig. 11. Effect of the mass amount on: (a) moment demand distribution;
(b) shear demand distribution; (c) drift demand distribution

e) Reinforcement ratio

The values for shear and bending moment in the seismic design of the tested specimen met CSA A23.3 requirements which uses capacity design and presumes that plasticity does not spread into the upper portions of the walls [22]. Nonlinear dynamic analysis revealed that the plasticity developed in the upper level of the wall even though it had been designed for plastic hinge formation only at the base. The experimental results of Ghorbanirenani et al. [28] and numerical modeling results indicate that inelastic behavior can spread to the upper regions.

Figure 12 shows the effect of longitudinal reinforcement ratio on wall response. Doubling and tripling the longitudinal reinforcement increased the base moment about 53% and 69% and the base shear about 54% and 62%, respectively. Utilizing one-half the longitudinal reinforcement decreased the base moment and shear about 22% and 26%, respectively. The figure shows drift along the height of the wall with different ratio of longitudinal reinforcement.
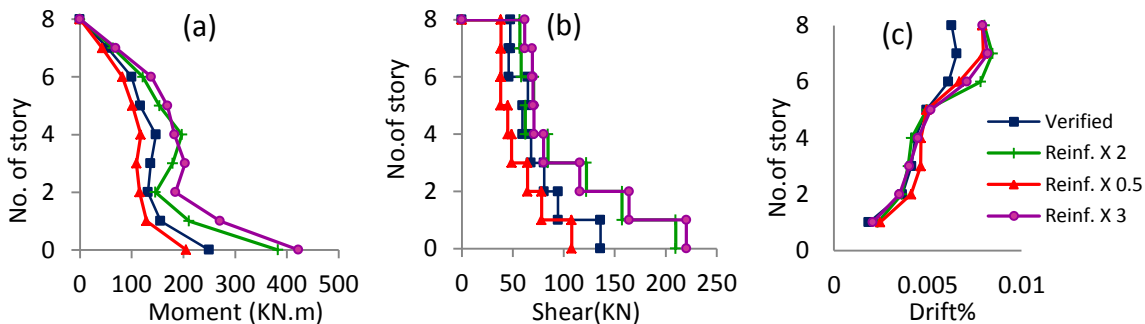

Fig. 12. Effect of longitudinal reinforcement ratio along the wall height on: (a) moment demand
distribution; (b) shear demand distribution; (c) drift demand distribution

Doubling and tripling longitudinal reinforcement did not affect first and sixth story rotation significantly (Table 1). In fact, the yield curvature and yield rotation were not a function of flexural resistance or reinforcement ratio.

f) Concrete strength

The concrete module of elasticity (E_c) depends on the compression strength and it was 30 MPa from test. In the numerical model, the concrete strengths of 30, 45 and 60 MPa were examined and it was found that the effect of increased concrete strength on the moment was not significant (Fig. 13).

g) Upper-level reinforcement

The idea of increasing the longitudinal reinforcement ratio in the upper levels was tested to maintain these levels in the elastic range. Longitudinal reinforcement of the first and second stories was kept constant and the longitudinal reinforcement ratio of the upper stories was increased two- and three-fold.

Figure 14 plots the results for bending moment, shear and drift demands. The base moment demand remained approximately constant in these models. It can be concluded that flexural hinging in the upper segment of the wall can be used to control the force demanded by higher mode responses and that keeping this region in the elastic range may not be a realistic technical and economic solution.
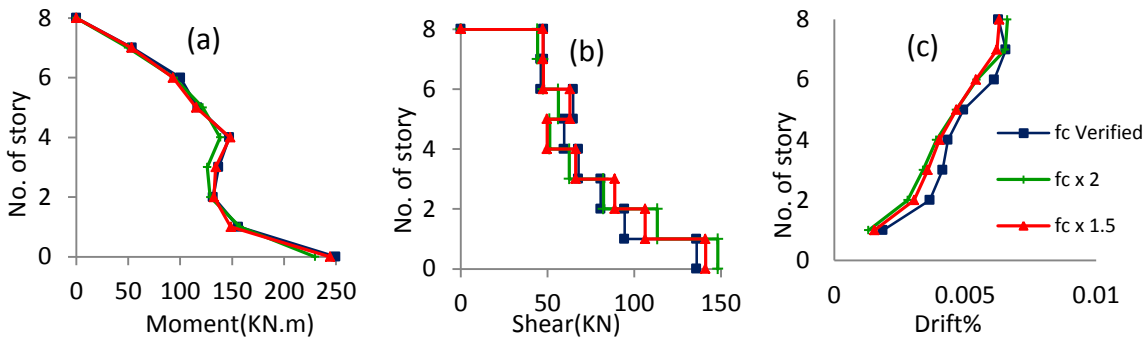

Fig. 13. Effect of concrete compression strength on: (a) moment demand distribution;
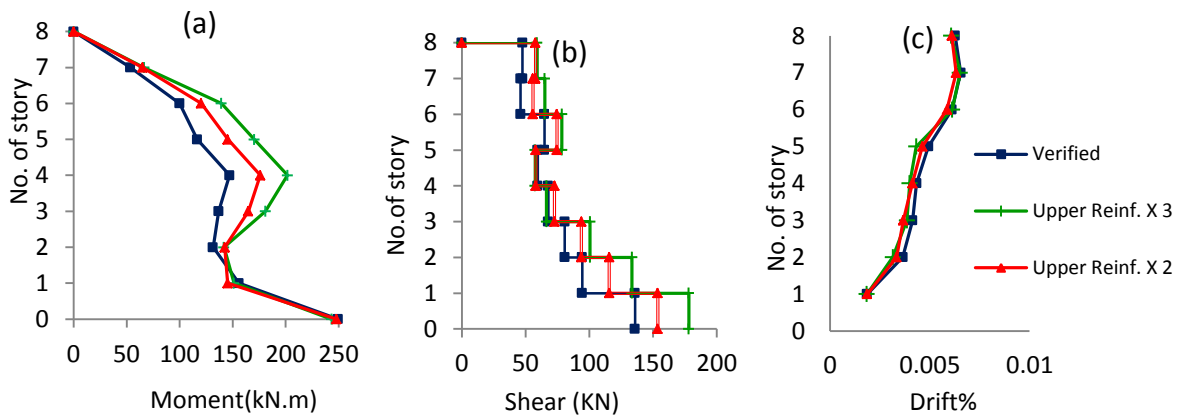(b) shear demand distribution; (c) drift demand distribution

Fig. 14. Effect of longitudinal reinforcement ratio at the levels upper than the base level on: (a) moment demand distribution; (b) shear demand distribution; (c) drift demand distribution

6. CONCLUSION

The present study examined the nonlinear dynamic behavior of shear walls and the effect of numerical modeling assumptions and parameters on the responses. A nonlinear fiber model was prepared to represent a large-scale 8-story RC shear wall subjected to shaking table testing. Nonlinear time history analysis was performed and the following conclusions and recommendations were drawn:

1. The results showed that slender shear walls subjected to design-level base motions can experience an inelastic flexural response in their upper levels. The development of plasticity into these regions in response to the effect of higher modes was captured using a nonlinear fiber element model. Nonlinear behavior of the upper levels mitigated seismic demand along the height.

2. The overall responses of the verified fiber model were in good agreement with the experimental results, including those for moment, shear and drift distribution envelopes, rotation and top horizontal displacement.

3. An investigation of effective shear stiffness showed that utilizing $(\frac{Gc.Ag}{20})$ in the sixth and seventh stories and $(\frac{Gc.Ag}{7})$ in the other stories produced a reasonable shear force demand distribution envelope, which is in agreement with the experimental results. Different values for shear stiffness did not appreciably affect moment demand.

4. Utilizing 2.5% Modal damping plus 0.15% Rayleigh damping for all modes produced the best agreement between the numerical and experimental results. Moment demands were moderately sensitive to Modal damping. Shear demand and drift demand were more sensitive. For example, decreasing the Modal damping ratio from 2.5% to 1% increased upper level drift about 45%.

5. The sole use of Rayleigh damping in the models did not produce agreement between numerical responses and experimental results. For example, 2.5% Rayleigh damping, which is typical for tall buildings, resulted in upper level rotation of about one-half the actual rotation at these levels.

6. Increasing the axial load increased the moment and shear demand. For instance, increasing the axial load ratio from 2.7% to 18% increased the base moment and base shear by about 73% and 60%, respectively. This is a result of increased moment capacity in response to the increase in axial load. No consistent rule was found for drift versus axial loading.

7. Doubling and tripling the longitudinal reinforcement ratio increased the base moment about 53% and 69%, respectively. Utilizing one-half the longitudinal reinforcement decreased the base moment about 22%. These values were roughly equivalent to those for base shear. Increasing longitudinal reinforcement did not mitigate story drift and increased flexural demand, so that rotation remained approximately unchanged. Yielding rotation was not a function of moment resistance; increasing the longitudinal reinforcement did not appreciably change this value. It was demonstrated that doubling and tripling the reinforcement did not prevent the spread of plasticity to the upper levels.

8. Tripling the longitudinal reinforcement in the upper stories while keeping the first- and second- story longitudinal reinforcement constant increased mid-height moment and base shear demands about 38% and 30%, respectively.

REFERENCES

1. Kaplan, H., Gönen, H., Nohutcu, H., Çetinkaya N. & Yilmaz, S. (2009). A new strong floor-reaction wall system without gallery for experimental studies in structural mechanics. *Iranian Journal of Science and Technology, Transaction B: Engineering*, Vol. 33, No. B4.

2. Kheyroddin, A. & Naderpour, H. (2008). Nonlinear finite element analysis of composite RC shear walls. *Iranian Journal of Science and Technology, Transaction B: Engineering*, Vol. 32, No. B2.

3. Kheyroddin, A., Naderpour, H., Ghodrati Amiri, G. & Hoseini Vaez, S. R. (2011). Influence of carbon fiber reinforced polymers on upgrading shear behavior of RC coupling beams. *Iranian Journal of Science & Technology, Transactions of Civil Engineering*, Vol. 35, No. C2.

4. Seren Akavci, S. (2007). Nonlinear analysis of semi-rigid frames with rigid end sections. *Iranian Journal of Science and Technology, Transaction B: Engineering*, Vol. 31, No. B5.

5. Hajirasouliha, I. & Doostan, A. (2010). A simplified model for seismic response prediction of concentrically braced frames. *Advances in Engineering Software*, Vol. 41, pp. 497–505.

6. Arslan, H. M., Aksogan, O. & Choo, B. S. (2004). Free vibrations of flexibly connected elastically supported stiffened coupled shear walls with stepwise changes in width. *Iranian Journal of Science and Technology, Transaction B: Engineering*, Vol. 28, No. B5.

7. Orakcal, K. & Wallace, J. W. (2006). Flexural modeling of reinforced concrete walls – model calibration. *ACI Structural Journal,* Vol. 103, No. 2, pp. 196–206.

8. Schotanus, M. I. & Maffei, J. R. (2008). Computer modeling and effective stiffness of concrete wall buildings. *Tailor Made Concrete Structures*, eds. J. Walraven and D. Stoelhorst (Taylor & Francis Group, London).

9. Grange, S., Kotronis, P. & Mazars, J. (2009). Numerical modeling of the seismic behaviour of 7-story building: NEES benchmark. *Materials and Structure,* Vol. 42, No. 10, pp. 1433–1442.

10. Kim, Y., Kabeyasawa, T., Matsumori, T., & Kabeyasawa, T. (2011). Numerical study of a full-scale six-storey reinforced concrete wall-frame structure tested at E-Defense. *Earthquake Engineering & Structural Dynamics,* Vol. 41, No. 8, pp. 1217–1239.

11. Wallace, JW. (2007). Modelling issues for tall reinforced concrete core wall buildings. *The Structural Design of Tall and Special Buildings,* Vo. 16, No. 615–632.

12. PERFORM-3D. (2006). *Nonlinear analysis and performance assessment for 3D structures.* Version 4, Computer & Structures Inc.: Berkeley, CA.

13. Seismosoft. SeismoStruct – (2009). A computer program for static and dynamic nonlinear analysis of framed structures. Available from <http://www.seismosoft.com.

14. Yang, T. Y., Moehle, J. P., Bozorgnia, Y., Zareian, F. & Wallace, J. W. (2012). Performance assessment of tall concrete core-wall building designed using two alternative approaches. *Earthquake Engineering & Structural Dynamics*, Vol, 41, pp.1515–1531.

15. Beiraghi, H., Kheyroddin, A. & Kafi, M. A. (2015). Forward directivity near-fault and far-fault ground motion effects on the behavior of reinforced concrete wall tall buildings with one and more plastic hinges. *The Structural Design of Tall and Special Buildings*, Article first published online: 29 DEC 2015 (under press). doi:10.1002/tal.1270.

16. Munir, A. & Warnitchai, P. (2012). The cause of unproportionately large higher mode contributions in the inelastic seismic responses of high-rise core-wall buildings. *Earthquake Engineering & Structural Dynamics*, Vol. 41, pp. 2195–2214.

17. 113 Klemencic, R., Fry, J. A., Hooper, J. D. & Morgen, B G. (2007). Performance-based design of ductile concrete core wall buildings—issues to consider before detailed analysis. *The Structural Design of Tall and Special Buildings*, Vol. 16, No. 5, pp. 599–614.

18. Zekioglu, A., Willford, M., Jin, L. & Melek, M. (2007). Case study using the Losangeles tall buildings structural design council guidelines: 40-storey concrete core wall building. *The Structural Design of Tall and Special Buildings*, Vol. 16, No. 5, pp.583–597.

19. Gonzales, H., & López-Almansa, F. (2012) Seismic performance of buildings with thin RC bearing walls. *Engineering Structures*, Vol. 34, pp. 244–258

20. Orakcal, K., Conte, J.P. & Wallace, J. W. (2004). Flexural modeling of reinforced concrete walls − model attributes. *ACI Structural Journal,* Vol. 101, No. 5, pp. 688–698.

21. Luu, H., Ghorbanirenani, I., Léger, P. & Tremblay, R. (2013). Numerical Modeling of Slender Reinforced Concrete Shear Wall Shaking Table Tests Under High-Frequency Ground Motions. *Journal of Earthquake Engineering*, Vol.17, No. 4, pp. 517-542.

22. Paulay, T. & Priestley, M. J. N. (1992). *Seismic design of reinforced concrete and masonry buildings*. Wiley: Hoboken, NJ.

23. CSA Standard A23.3-04. (2005) *Design of Concrete Structures*. Canadian Standard Association: Rexdale, Canada, p. 214.

24. NZS 3101. (2006). *New Zealand Standard, Part 1—The Design of Concrete Structures*. Standards New Zealand, Wellington, New Zealand.

25. CEN EC8.*(2004). Design of Structures for Earthquake Resistance*. European Committee for Standardization: Brussels, Belgium.

26. Rodriguez, M. E. & Restrepo, J. I. & Carr, A. J. (2002). Earthquake-induced floor horizontal accelerations in buildings. *Earthquake Engineering and Structural Dynamics*, Vol. 31, pp. 693–718.

27. Panneton, M., L´eger, P. & Tremblay, R. (2006). Inelastic analysis of a reinforced concrete shear wall building according to the national building code of Canada 2005. *Canadian Journal of Civil Engineering*, Vol. 33, pp. 854–871.

28. Priestley, M. J. N., Calvi, G. M. & Kowalsky, M. J. (2007). *Displacement based seismic design of structures*, IUSS Press: Pavia, Italy, 2007.

29. Ghorbanirenani, I., Tremblay, R., Léger, P. & Leclerc, M. (2012). Shake Table Testing of Slender RC Shear Walls Subjected to Eastern North America Seismic Ground Motions. *Journal of Structural Engineering*, Vol. 138, No.12, pp. 1515-1529.

30. NRCC. (2005). *National building code of Canada*. 12th ed, National Research Council of Canada, Ottawa, ON, Canada.

31. Panagiotou, M. & Restrepo, J. I. (2009). Dual-plastic hinge design concept for reducing highermode effects on high-rise cantilever wall buildings. *Earthquake Engineering & Structural Dynamics*, Vol. 38, No. 12, pp. 1359–1380.

32. Hidalgo, P. A., Jordan, R. M. & Martinez, M. P. (2002). An analytical model to predict the inelastic seismic behavior of shear-wall, reinforced concrete structures. *Engineering Structures,* Vol. 24, pp. 85–98.

33. Applied Technology Council. (2010). ATC-72: *Modeling and acceptance criteria for seismic design and analysis of tall buildings*. ATC, Redwood City, CA.

34. Powell, G. (2010). *Modeling for structural analysis*. Computers and Structures, Inc., Berkeley, CA, Ed.

35. Kent, D. & Park, R. (1971). Flexural member with confined concrete. *Journal of Structural Division, Proc. of the American Society of Civil Engineers,* Vol. 97, No. ST7, pp. 1969–1990.

36. PERFORM-3D. (2006). Nonlinear Analysis and Performance Assessment for 3D Structures, V.4, User Guide. Computers and Structures, Inc., (CSI), Berkeley, CA.

37. Ghodsi, T., Ruiz, J. F., Massie, C. & Chen, Y. (2010). Pacific earthquake engineering research/seismic safety commission tall building design case study. *The Structural Design of Tall and Special Buildings*, Vo1.9, pp.197-256.

38. Priestley, M. J. N. & Grant, D. N. (2005). Viscous damping in seismic design and analysis. *Journal of Earthquake Engineering*, Vol. 9, No. SP2, pp. 229-255.

39. Léger, P. & Dussault, S. (1992). Seismic-energy dissipation in MDOF structures. *Journal of Structural Engineering*, Vol. 118, No. 5, pp. 1251–1269.

40. Smyrou, E., Priestley, M. J. N. & Carr, A. J. (2011). Modelling of elastic damping in nonlinear time-history analyses of cantilever RC walls. *Bulletin of Earthquake Engineering,* Vol. 9, pp. 1559–1578.

41. Chopra, A. K. (2001). *Dynamics of structures*. Prentice-Hall, New Jersey.

42. PERFORM-3D. (2006). *Nonlinear analysis and performance assessment for 3D structures*, V.4, User Guide. Computers and Structures, Inc., (CSI), Berkeley, CA.

43. Park, R. & Paulay, T. (1975). *Reinforced concrete structures*. Wiley: Hoboken, NJ, 1975.